

Jin Wei · Dengqing Cao · Hua Huang · Lianchao Wang ·
Wenhu Huang

Dynamics of a multi-beam structure connected with nonlinear joints: modelling and simulation

Received: 6 September 2017 / Accepted: 28 February 2018 / Published online: 9 March 2018
© Springer-Verlag GmbH Germany, part of Springer Nature 2018

Abstract A dynamic modelling approach for a multi-beam structure connected with nonlinear joints is presented and subsequently used to obtain its reduced-order analytical model. Firstly, by applying the matching and boundary conditions, the natural frequencies and global mode shapes of the system are derived. According to the nonlinear transmitted torque formulations of the joints, the joints nonlinearities are introduced into the system by using the equilibrium conditions between the beams and the joints. Then, the global mode shapes and their orthogonality relations are used to obtain an explicit set of reduced-order nonlinear ordinary differential equations (ODEs) of motion for the flexible structure with nonlinear joints. A flexible structure composed of 4 beams and nonlinear joints is given as an example to illustrate the application of the modelling approach proposed. And a comparison between the natural frequencies obtained by the proposed approach and those from the finite element method is given to verify the validity of the derived model. Through the nonlinear ODEs obtained by the Galerkin truncation of the original dynamic model, a study on the variation in dynamic responses of the system with different numbers of modes is performed. The results are used to determine the number of modes taken in nonlinear vibration analysis for certain range of the vibration amplitude of the external excitation. The dynamic responses of the system with various joint parameters are worked out, which show that the transmission characteristics of the joints can strongly affect the dynamic behavior of the whole structure.

Keywords Multi-beam structure · Nonlinear joints · Dynamic modelling · Reduced-order model · Nonlinear dynamic behavior

1 Introduction

A specific structure composed of multiple flexible beams and flexible joints is widely used in the fields of aerospace and civil engineering, such as the solar array and large truss structure. Due to the strong nonlinearities of the joints, complex micromechanical phenomena under the effect of applied loadings may be produced. This makes the dynamic behavior of the whole structure become more complicated. Therefore, an understanding of the dynamic characteristics of such systems is essential for their design and control of vibration.

A first step toward investigating the dynamic behavior of these structural systems must be intended to understand how to describe the relationship between load and deformation in a dynamic model of the joint. Based on the Hertz contact theory [1–6], the joint can be described as a spring damping system in terms of the

J. Wei · D. Cao (✉) · L. Wang · W. Huang
School of Astronautics, Harbin Institute of Technology, PO Box 137, Harbin 150001, China
E-mail: dqcao@hit.edu.cn

H. Huang
China Academy of Space Technology, Beijing 100094, China

contact force and deformation. According to the relative velocity of the contact, the geometry of the contact surface and the properties of the material and the contact duration, many scholars have proposed a variety of contact force models which have been used to investigate the dynamic behavior of contact and collision in a mechanical system with joint clearance. On the other hand, an alternative approach for establishing a theoretical model of the joint is to extract the model parameters from experimental data using joint identification techniques [7–12]. Crawley [8,9] developed a force-state mapping technique to measure the parameters of the joint, where the force transmitted by the joint is represented as the function of the full mechanical state of the joint.

For these structures with numerous joints, there have been some research on the overall dynamics of the structure considering the effects of the joints characteristics [13–21]. Bowden [19] formulated the equations of motion for the three-joint beam model and investigated the effect of three cubic nonlinear stiffness and linear damping of the joint on the global dynamics of the jointed structures in Ref [14], which shows the interesting relationship between linear properties of the system, such as resonant-free frequencies and joint participation, and nonlinear system properties, such as the shape of the backbone curves. The dynamic behavior of multi-degree-of-freedom flexible jointed structures is then analyzed in Sarkar [18] using a Fourier–Galerkin algorithm. Further studies on the dynamic formulation of jointed space structures have been presented in Tomihiko [17] and Zhang et al [21]. For the practical engineering problems, the dynamic analysis of the structure is usually carried out by the finite element model of the spacecraft structure. Wei and Zheng [20] investigated the nonlinear vibration of satellites with joint nonlinearities by using an improved frequency domain method, which is applicable to large-scale and complicated finite element models.

In the case of modelling of complex flexible multi-body structures, the structural complexity and full coupling result in a model with a great many DOFs and strong nonlinearity, which also bring a challenge for the design of control laws. In order to derive a low-dimensional model for the flexible structure, an effective technique for converting the continuous system into an equivalent discrete system is to use the mode functions [22]. Compared to FEM, the method of using the mode functions to discrete continuous system can greatly reduce the DOFs of the system, which is very suitable for the controller design. However, the accuracy of the dynamic model is highly dependent on how truthful the adopted mode functions can represent the real deformations of the system. For the multi-beam structure connected with flexible joints, due to the interactions of the beams and flexible joints, it is difficult to select the appropriate mode functions to discretize the system when using the assumed mode method. Recently, Wei et al [23] proposed an analytical method to obtain the global mode shapes, which are used to truncate the PDEs of the system to the ODE with a few DOFs. Through the simulation examples for the manipulator system, it shows that the model derived by this method has a relatively high accuracy in comparison with those using the assumed mode method. Therefore, for the multi-beam structure, it is very suitable to use the global modes to obtain the dynamic model of the system, because the global modes obtained by this method are accurate and can represent the real deformations of the system.

For the multi-body structure of spacecraft in orbit, the damping and nonlinearity in the joints are much higher than those produced by other factors such as structural material and geometric large deformations, which makes that the joints become the dominant sources of damping and nonlinearities of the whole structure [24]. Meanwhile, the damping and nonlinearity in the joints are not continuously distributed throughout the whole structure but occur at discrete locations. This brings difficulties to the establishment of the accurate model of the system. In this paper, according to the nonlinear transmitted torque formulations of the joints, the joints nonlinearities are introduced into the system by using the equilibrium conditions between the beams and the joints. Thus, an explicit set of reduced-order nonlinear ODEs are obtained for the multi-beam structure considering the joints nonlinearities by using the global modes discretization technique. Furthermore, the reduced-order nonlinear ODEs are put into a form which is convenient for an analytical investigation to predict nonlinear phenomena exhibited by this structure.

In this article, the natural frequencies and the corresponding global mode shapes of the whole system are obtained by the method proposed in Refs [23,25–27]. Through the nonlinear transmitted torque formulations of the joints, the joint nonlinearities are introduced into the system by using the equilibrium conditions between the beams and the joints. In this way, the global mode shapes and their orthogonality relations are used to obtain an explicit set of reduced-order nonlinear ODEs of motion for the structure with nonlinear joints. Then, an application example of such structure is presented to illustrate the use of the presented approach. Based on the application example, a comparison of the natural frequencies is given to verify the validity of the derived model. Through the dynamic equations presented in the example, the dynamic responses of the system with different numbers of modes are studied, and the dynamic responses of the system with various joint parameters are performed to investigate the effect of the nonlinear joints.

2 Dynamic modelling for a flexible structure with nonlinear joints

2.1 Governing equations of motion

Consider the planar motion of a flexible structure that consists of a number of beams and torsional joints, as shown in Fig. 1. The beams are connected by the torsional joints. The length, mass per unit length, elastic modulus and area moment of inertia of the i th beam b_i are denoted by $2l_i$, ρ_i , E_i and I_i , respectively. θ_i is used to describe the torsional deformation of the i th joint S_i . Let (x_i, y_i) be the local coordinates of the beam b_i in the vertical plane, with the origin located in the middle of the beam b_i .

The Euler–Bernoulli beam theory is used to derive the equation [28] of motion for the i th beam

$$\rho_i \ddot{w}_i + \xi_i \dot{w}_i + E_i I_i w_i'''' + \eta_i I_i \dot{w}_i''' = 0, \quad i = 1, 2, \dots, N, \tag{1}$$

where an overdot denotes partial differentiation with respect to time t , a prime denotes partial differentiation with respect to x_i , w_i is the vertical displacement of the i th beam, ξ_i and η_i are the external and internal damping coefficient of the i th beam, respectively.

As shown in Fig. 2, the torsional joint is described as a single-degree-of-freedom massless system with a nonlinear spring and a linear damper. Based on the parameter identification method, the torque transmitted by the joint can be represented as the function of the instantaneous state of the joint. Then, the nonlinear transmitted torque formulation [9] of the i th joint can be expressed as

$$M_i^T = c_i \dot{\theta}_i + k_i^L \theta_i + k_i^N \theta_i^3 + \mu_i \text{sign}(\dot{\theta}_i), \tag{2}$$

where the first three terms of Eq. (2) represent a linear damping, a linear spring and a third-order nonlinear spring, respectively, and the last term represents Coulomb friction. c_i , k_i^L , k_i^N and μ_i are linear damping coefficient, linear spring stiffness coefficient, third-order spring stiffness coefficient and Coulomb friction torque of the i th joint S_i , respectively.

To complete the formulation for the boundary value problem of the system, one must specify the matching conditions at the joints S_1, S_2, \dots, S_{N-1} and the boundary conditions at the free ends A and B . As shown in Fig. 3a, the geometric matching conditions at the joint $S_j (j = 1, 2, \dots, N - 1)$ can be written as

$$w_j(l_j, t) = w_{j+1}(-l_{j+1}, t), \tag{3}$$

$$w_j'(l_j, t) + \theta_j = w_{j+1}'(-l_{j+1}, t). \tag{4}$$

As shown in Fig. 3b, the torsional joint S_j is subjected to the shear forces and bending moments of the beams b_j and b_{j+1} , respectively. The force and moment matching conditions at the joint S_j are

$$E_j I_j w_j'''(l_j, t) = E_{j+1} I_{j+1} w_{j+1}'''(-l_{j+1}, t), \tag{5}$$

$$E_j I_j w_j''(l_j, t) = M_j^T = E_{j+1} I_{j+1} w_{j+1}''(-l_{j+1}, t). \tag{6}$$

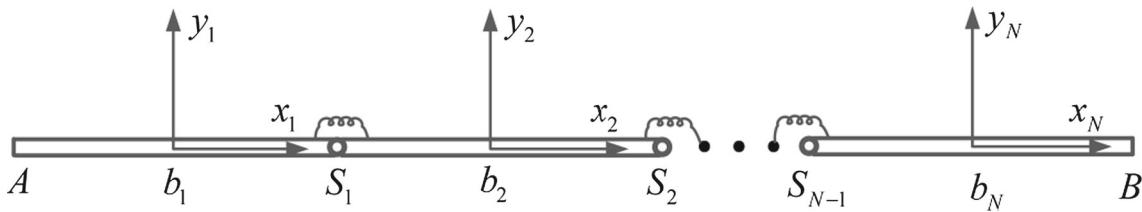


Fig. 1 Schematic of the flexible structure connected with nonlinear joints

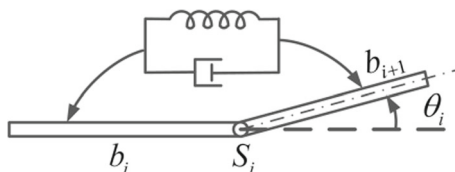


Fig. 2 Schematic of the joint model

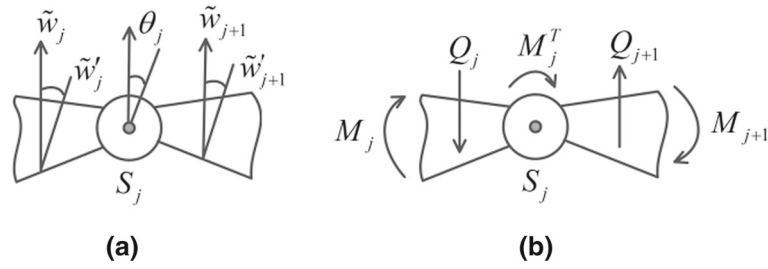


Fig. 3 Schematic of the **a** geometric and **b** force matching conditions at the torsional joint; $\tilde{w}_j = w_j(l_j, t)$, $\tilde{w}_{j+1} = w_{j+1}(-l_{j+1}, t)$, $\tilde{w}'_j = w'_j(l_j, t)$, $\tilde{w}'_{j+1} = w'_{j+1}(-l_{j+1}, t)$, θ_j describes the torsional deformation of the j -th torsional joint, Q_j and Q_{j+1} are the shear forces acting on the left and right sides of the j -th torsional joint, $Q_j = E_j I_j w''_j(l_j, t)$, $Q_{j+1} = E_{j+1} I_{j+1} w''_{j+1}(-l_{j+1}, t)$, M_j and M_{j+1} are the bending moments acting on the left and right sides of the j -th torsional joint, $M_j^T = M_j = E_j I_j w''_j(l_j, t)$, $M_{j+1}^T = M_{j+1} = E_{j+1} I_{j+1} w''_{j+1}(-l_{j+1}, t)$

The boundary conditions at A and B are

$$A : E_1 I_1 w_1'''(-l_1, t) = 0, E_1 I_1 w_1''(-l_1, t) = 0, \tag{7}$$

$$B : E_N I_N w_N'''(l_N, t) = 0, E_N I_N w_N''(l_N, t) = 0. \tag{8}$$

2.2 Determination of natural frequencies and global mode shapes

In order to obtain a low-dimensional dynamic model, it is necessary to study the eigenvalue problem of the system to obtain the global mode shapes. Therefore, it is assumed that the displacements of the flexible structure are separable in space and time to solve the eigenvalue problem of the system. Let

$$w_i(x_i, t) = \varphi_i(x_i)e^{j\omega t}, \theta_i = \Theta_i e^{j\omega t}, \tag{9}$$

where ω is an unknown constant corresponding to the natural frequency of the system. Substituting the separable solutions given in Eq. (9) into Eq. (1) without damping yields

$$E_i I_i \varphi_i''''(x_i) - \omega^2 \rho_i \varphi_i(x_i) = 0, \quad i = 1, 2, \dots, N. \tag{10}$$

The solutions of Eq. (10) can be written as

$$\varphi_i(x_i) = A_i \cos(\beta_i x_i) + B_i \sin(\beta_i x_i) + C_i \cosh(\beta_i x_i) + D_i \sinh(\beta_i x_i), \quad x_i \in [-l_i, l_i], \tag{11}$$

where $\beta_i = \left(\frac{\rho_i \omega^2}{E_i I_i}\right)^{1/4}$. Let

$$\Psi_i = [A_i \ B_i \ C_i \ D_i \ \Theta_i], \Psi = [\Psi_1 \ \Psi_2 \ \dots \ \Psi_N]^T. \tag{12}$$

Substituting Eq. (11) into the linearized matching conditions (3)–(6) and boundary conditions in (7) and (8) yields

$$\mathbf{H}(\omega)\Psi = 0, \tag{13}$$

where the matrix $\mathbf{H}(\omega) \in R^{(5N-1) \times (5N-1)}$.

The positive roots of the frequency equation $\det(\mathbf{H}(\omega)) = 0$, denoted in ascending order by $\omega_1, \omega_2, \dots$, are the natural frequencies of the linearized dynamic model of the structure. The eigenvector $\Psi^{(s)}$, where $s = 1, 2, \dots$, corresponding to the natural frequency ω_s can be obtained by Eq. (13). Once the natural frequency ω_s and the corresponding vector $\Psi^{(s)}$ are obtained, the s th mode shapes for the flexible structure can be determined by Eq. (11).

2.3 Orthogonality of the global mode shapes

The global mode shapes associated with the two distinct eigenvalues ω_r and ω_s are denoted by $\phi_r(x)$ and $\phi_s(x)$, respectively, where

$$\phi_r(x) = [\varphi_1^r \varphi_2^r \cdots \varphi_N^r]^T, r = 1, 2, \dots \tag{14}$$

By Eq. (10), one has

$$E_i I_i \varphi_i^{r''''}(x_i) = \omega_r^2 \rho_i \varphi_i^r(x_i). \tag{15}$$

Then, multiply Eq. (15) by φ_i^s and integrate the resulting equations over the domain $-l_i \leq x_i \leq l_i$ for the i th beam, and add the resulting equations to get

$$\sum_{i=1}^N \int_{-l_i}^{l_i} E_i I_i \varphi_i^{r''''}(x_i) \varphi_i^s(x_i) dx_i = \omega_r^2 \sum_{i=1}^N \int_{-l_i}^{l_i} \rho_i \varphi_i^r(x_i) \varphi_i^s(x_i) dx_i. \tag{16}$$

Integrating Eq. (16) by parts, using the matching and boundary conditions in Eqs. (3)~(8), yields

$$\sum_{i=1}^N \int_{-l_i}^{l_i} E_i I_i \varphi_i^{r''''}(x_i) \varphi_i^s(x_i) dx_i = \sum_{i=1}^N \int_{-l_i}^{l_i} E_i I_i \varphi_i^{r''}(x_i) \varphi_i^{s''}(x_i) dx_i + \sum_{i=1}^{N-1} k_i^L \Theta_i^r \Theta_i^s. \tag{17}$$

Substituting Eq. (17) into the left-hand side of Eq. (16) yields

$$\omega_r^2 \sum_{i=1}^N \int_{-l_i}^{l_i} \rho_i \varphi_i^r(x_i) \varphi_i^s(x_i) dx_i = \sum_{i=1}^N \int_{-l_i}^{l_i} E_i I_i \varphi_i^{r''}(x_i) \varphi_i^{s''}(x_i) dx_i + \sum_{i=1}^{N-1} k_i^L \Theta_i^r \Theta_i^s. \tag{18}$$

Exchanging the superscripts s and r in Eq. (18) yields

$$\omega_s^2 \sum_{i=1}^N \int_{-l_i}^{l_i} \rho_i \varphi_i^r(x_i) \varphi_i^s(x_i) dx_i = \sum_{i=1}^N \int_{-l_i}^{l_i} E_i I_i \varphi_i^{r''}(x_i) \varphi_i^{s''}(x_i) dx_i + \sum_{i=1}^{N-1} k_i^L \Theta_i^r \Theta_i^s. \tag{19}$$

Subtracting Eq. (19) from Eq. (18) yields

$$(\omega_r^2 - \omega_s^2) \sum_{i=1}^N \int_{-l_i}^{l_i} \rho_i \varphi_i^r(x_i) \varphi_i^s(x_i) dx_i = 0. \tag{20}$$

From Eq. (20), the first orthogonality relation can be obtained

$$\sum_{i=1}^N \int_{-l_i}^{l_i} \rho_i \varphi_i^r(x_i) \varphi_i^s(x_i) dx_i = M_s \delta_{rs}, \tag{21}$$

where M_s is a positive constant and δ_{rs} is the Kronecker delta. Using Eqs. (18) and (21), the second orthogonality relation can be obtained

$$\sum_{i=1}^N \int_{-l_i}^{l_i} E_i I_i \varphi_i^{r''}(x_i) \varphi_i^{s''}(x_i) dx_i + \sum_{i=1}^{N-1} k_i^L \Theta_i^r \Theta_i^s = K_s \delta_{rs}, \tag{22}$$

where K_s is a positive constant.

2.4 Dynamic model with multi-DOF

Applying the Galerkin procedure to Eqs. (1) and (2), the reduced-order nonlinear ODEs are obtained for the system. By using the first n global mode shapes, the displacements of the system can be written as

$$w_i(x_i, t) = \sum_{j=1}^n \varphi_i^j(x_i)q_j(t), \theta_i = \sum_{j=1}^n \Theta_i^j q_j(t), \tag{23}$$

where $q_j(t)$ is a modal coordinate.

Substituting Eq. (23) into Eqs. (1) and (2) yields

$$\sum_{j=1}^n \rho_i \varphi_i^j(x_i) \ddot{q}_j + \sum_{j=1}^n \xi_i \varphi_i^j(x_i) \dot{q}_j + \sum_{j=1}^n E_i I_i \varphi_i^{j''''}(x_i) q_j + \sum_{j=1}^n \eta_i I_i \varphi_i^{j''''}(x_i) \dot{q}_j = 0, \tag{24}$$

$$M_i^T = \sum_{j=1}^n c_i \Theta_i^j \dot{q}_j + \sum_{j=1}^n k_i^L \Theta_i^j q_j + \sum_{j=1}^n \sum_{k=1}^n \sum_{r=1}^n k_i^N \Theta_i^j \Theta_i^k \Theta_i^r q_j q_k q_r + \sum_{j=1}^n \mu_i \text{sign}(\Theta_i^j \dot{q}_j). \tag{25}$$

Multiplying Eq. (24) by φ_i^s , integrating the resulting equations over the domain $-l_i \leq x_i \leq l_i$ for the i th beam, adding all of the resulting equations and using the matching and boundary conditions in Eqs. (3)~(8) and the orthogonality relations in Eqs. (21) and (22), we have

$$M_s \ddot{q}_s + \left[\sum_{i=1}^N \sum_{j=1}^n \int_{-l_i}^{l_i} \xi_i \varphi_i^j(x_i) \varphi_i^s(x_i) dx_i + \sum_{i=1}^N \sum_{j=1}^n \int_{-l_i}^{l_i} \eta_i I_i \varphi_i^{j''''}(x_i) \varphi_i^s(x_i) dx_i + \sum_{i=1}^{N-1} \sum_{j=1}^n c_i \Theta_i^j \Theta_i^s \right] \dot{q}_j + K_s q_s + \sum_{i=1}^{N-1} \sum_{j=1}^n \mu_i \Theta_i^s \text{sign}(\Theta_i^j \dot{q}_j) + \sum_{i=1}^{N-1} \sum_{j=1}^n \sum_{k=1}^n \sum_{r=1}^n k_i^N \Theta_i^j \Theta_i^k \Theta_i^r q_j q_k q_r = 0, \quad s = 1, 2, \dots, n. \tag{26}$$

3 Example of application

Now, let us consider the solar array as an example of the multi-beam structure connected with nonlinear joints, as shown in Fig. 4. The solar array is composed of four solar panels connected by the torsional joints. Furthermore, the solar array is subjected to the external excitation due to the moving support. For a long solar array, it is appropriate to model the solar array as an assembly of the beams connected by the torsional joints

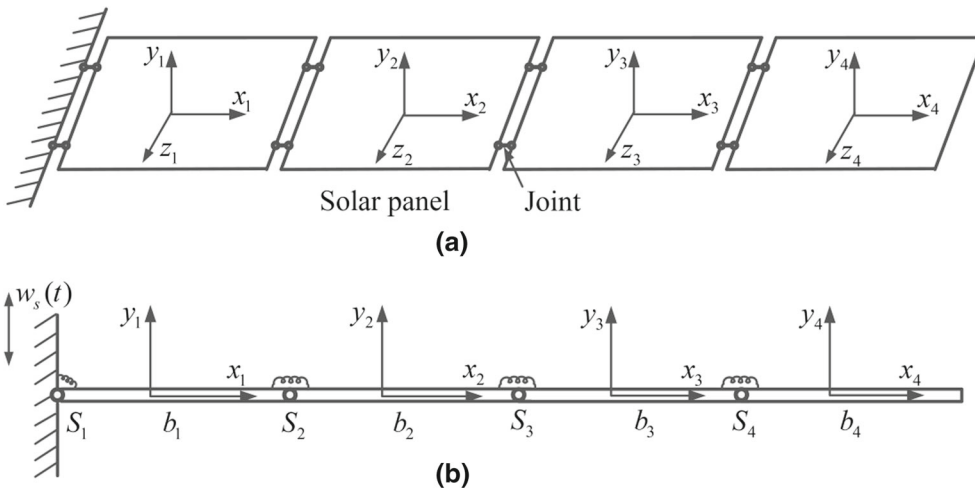


Fig. 4 Schematic of the solar array

Table 1 Values of the parameters of the solar array

Parameter	Value
Solar panel mass density ρ (kg/m)	1.64
Solar panel flexural rigidity EI (N m ²)	1493
Solar panel length $2l$ (m)	1.5
Solar panel external damping ξ (N s/m)	0.03
Solar panel internal damping η (N s/m ²)	1.9×10^5
Joint linear stiffness k_L (N m/rad)	2000
Joint third-order stiffness k_N (N m/rad ³)	1×10^7
Joint linear damping c (N m s/rad)	30
Joint Coulomb friction μ (N m)	0.2

[29]. In this example, the system is subjected to an excitation due to the moving support, as shown in Fig. 4b. Assume that the solar panels have the same dimensions of the cross section and material property. Similarly, the joints have the same geometric parameter and material property. For the sake of convenience, the subscripts of the corresponding symbols are removed, for example, $\rho_i = \rho$, $k_i^L = k_L$. The physical parameters of the array are listed in Table 1.

As shown in Fig. 4, the governing equation of motion for the i th beams is

$$\rho \ddot{w}_i + \xi \dot{w}_i + EI w''''_i + \eta I w''''_i = \rho \ddot{w}_s(t), \quad i = 1, 2, 3, 4, \quad (27)$$

where $w_s(t)$ is the displacement of the support.

Based on the dynamic modelling approach developed here, the nonlinear ODEs of motion for the system are obtained as follows:

$$\ddot{q}_s + \omega_s^2 q_s + 2\alpha_s \omega_s \dot{q}_s + \gamma_s \dot{q}_j + b_s^j \text{sign}(\Theta_i^j \dot{q}_j) + d_s^{jkr} q_j q_k q_r = f_s(t), \quad s = 1, 2, \dots, n, \quad (28)$$

where α_s is the modal damping ratio of the solar panels, γ_s is the damping of the joints, and b_s^j is the Coulomb friction torque of the joints. The relevant terms in Eq. (28) are given in ‘‘Appendix A’’.

4 Results and discussion

In this section, a comparison of the natural frequencies of the application example, which are obtained from the presented approach and the commercial software ANSYS, is performed. Then, the dynamic responses of the system with different numbers of modes are discussed, and the dynamic responses of the system with various joint parameters are given to investigate the effect of the nonlinear joints.

4.1 Model validation

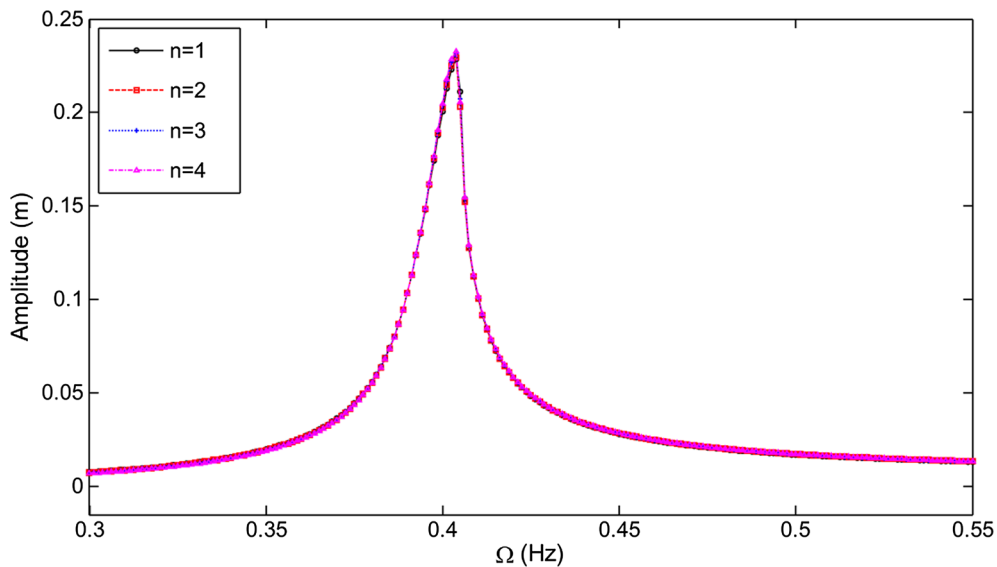
In order to verify the validity of the model as shown in Fig. 4, the first eight natural frequencies of the solar array with different joint linear stiffness are calculated by the proposed approach and compared with those obtained from the ANSYS, as shown in Table 2. Denote the dimensionless stiffness parameter of the joint by K_L , which defines the ratio between the linear torsional stiffness and the flexural rigidity of the solar panel, as

$$K_L = \frac{k_L l}{EI}. \quad (29)$$

The first eight natural frequencies obtained from the proposed approach and ANSYS for different K_L are listed in Table 2. It can be seen from Table 2 that the results from the proposed approach are in good agreement with those from the ANSYS. The maximum relative error between the natural frequencies from the current and finite element methods, defined by $(\|\omega_s - \omega_s^{\text{ANSYS}}\|)/\omega_s^{\text{ANSYS}}$, is 3.85%. This shows the correctness of the model obtained by this paper. Furthermore, Table 2 reveals that by increasing K_L , the natural frequencies increase, as expected.

Table 2 First eight natural frequencies of the solar array ω (Hz)

Mode	$K_L = 0.2$		$K_L = 1$		$K_L = 5$		$K_L = \infty$	
	ANSYS	Eq. (13)	ANSYS	Eq. (13)	ANSYS	Eq. (13)	ANSYS	Eq. (13)
1	0.265	0.273	0.386	0.398	0.438	0.452	0.474	0.470
2	1.653	1.710	2.375	2.473	2.727	2.823	2.970	2.940
3	4.609	4.773	6.631	6.869	7.593	7.877	8.338	8.231
4	8.571	8.901	12.66	13.09	14.74	15.28	16.41	16.13
5	23.45	23.10	24.78	24.71	25.90	26.03	27.27	26.67
6	31.68	31.32	34.91	35.33	37.51	38.43	40.96	39.83
7	42.79	42.43	47.92	48.69	51.92	53.44	57.52	55.63
8	53.39	53.23	61.58	63.15	68.05	70.50	76.98	74.67

**Fig. 5** Frequency-response curves of the solar array tip with different numbers of modes, $w_0 = 0.004$ m

4.2 Dynamic responses

To determine the number of modes taken for nonlinear vibration analysis, the forced harmonic responses of the system with different numbers of modes are worked out numerically, as shown in Figs. 5, 6, 7 and 8. The vertical displacement of the support is assumed as $w_s(t) = w_0 \cos \Omega t$. The first four natural frequencies of the system are $\omega_1 = 0.398$ Hz, $\omega_2 = 2.475$ Hz, $\omega_3 = 6.873$ Hz and $\omega_4 = 13.10$ Hz. The results are obtained from the cases with increasing Ω and w_0 . In these figures, the initial conditions for the first point are assumed to be zero, and some steady-state response data at the current Ω and w_0 are used as the initial conditions for the next Ω and w_0 , respectively.

When the external excitation frequency Ω varies from 0.3 to 0.55 Hz, the frequency response curves of the solar array tip with different numbers of modes for $w_0 = 0.004$, 0.01 and 0.012 m are shown in Figs. 5, 6 and 7, respectively. From these figures, it can be seen clearly that as w_0 is increased, the jump phenomenon is more obvious. Although the external excitation frequency is much smaller than the higher-order natural frequency of the system, the higher-order modes are needed to ensure the accuracy of the response of the system in the case of large vibration amplitude. This can be observed from the Figs. 6 and 7. For instance, the first two and three modes should be taken in dynamic models for $w_0 = 0.01$ and 0.012 m, respectively, so that the accuracy of nonlinear vibration analysis can be satisfied. It can be concluded that with the increase in the amplitude of the excitation, due to the effects of the joints nonlinearities, the contribution of the higher-order modes in the response of the system is increased. However, in the case of small vibration amplitude, the contribution of the higher-order modes in the response of the system can be ignored when the external excitation frequency is near the first linear natural frequency of the system. This can be observed from Fig. 5. At this time, the first mode is enough for the dynamic model, which makes that the dynamic equation presented in this paper is more

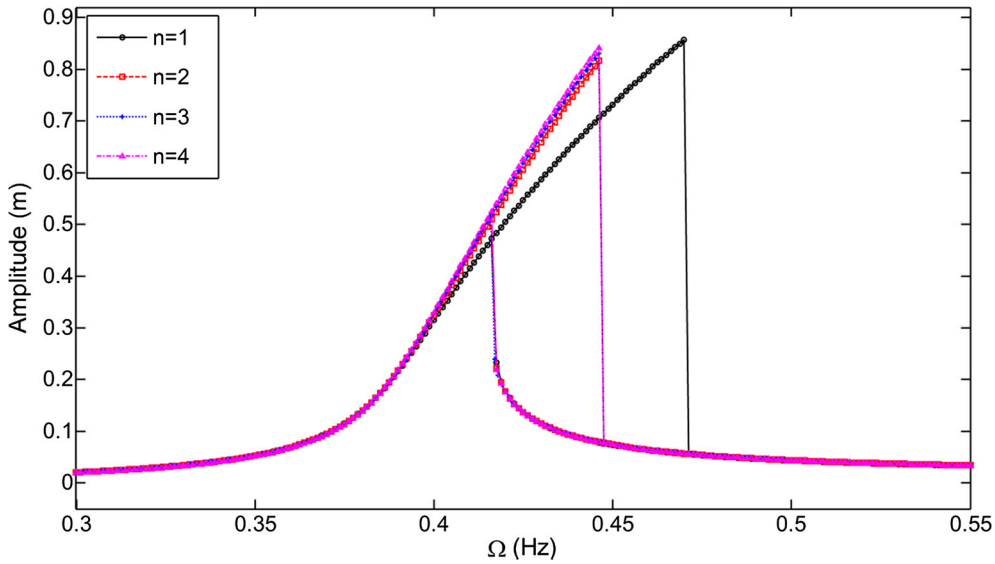


Fig. 6 Frequency-response curves of the solar array tip with different numbers of modes, $w_0 = 0.01$ m

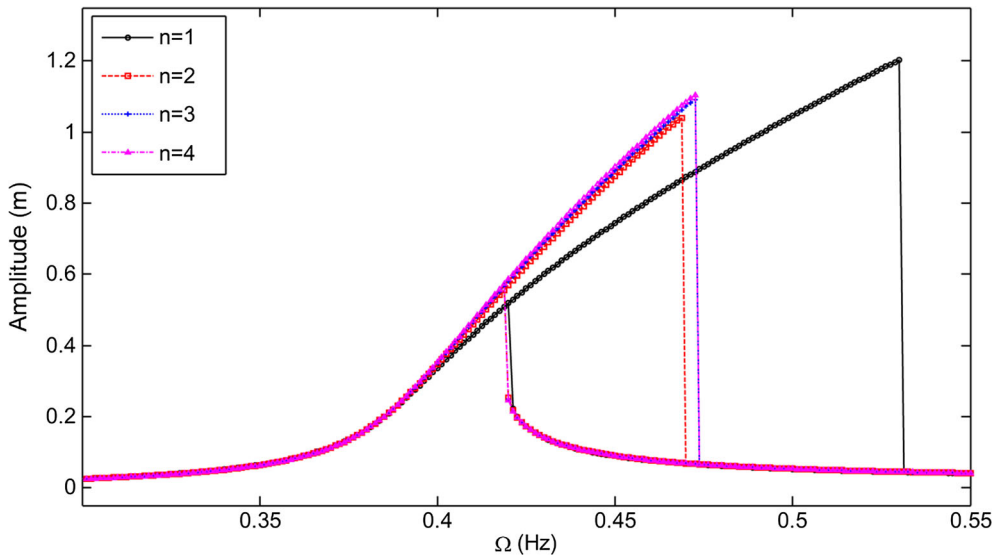


Fig. 7 Frequency-response curves of the solar array tip with different numbers of modes, $w_0 = 0.012$ m

convenient for solving the system with the analytic method, such as perturbation techniques. From Figs. 5, 6 and 7, it is concluded that how many modes should be taken for nonlinear vibration analysis depends on the amplitude of the excitation.

When the amplitude of the excitation w_0 is varied from 0.001 to 0.02 m, the force-response curves of the solar array tip with different numbers of modes for $\Omega = 0.42$ Hz are shown in Fig. 8. From Fig. 8, a similar jump phenomenon can be observed. With the increase in the amplitude of the excitation, the difference of the response curves with different numbers of modes becomes larger. All these clearly show that the contribution of the higher-order modes in the response of the system is closely related to the vibration amplitude of the system. This can also be observed from Figs. 5, 6 and 7.

From Figs. 5, 6, 7 and 8, it is found that when the vibration amplitude of the system is relatively large, more modes need to be taken to meet the requirements of accuracy. Therefore, in the next study on the effect of the joints nonlinearities on the system, the first three modes are selected to calculate the dynamic responses of the system. The forced harmonic responses of the system with various joint parameters are worked out numerically, as shown in Figs. 9, 10, 11, 12, 13 and 14. In these figures, the initial conditions for the first point

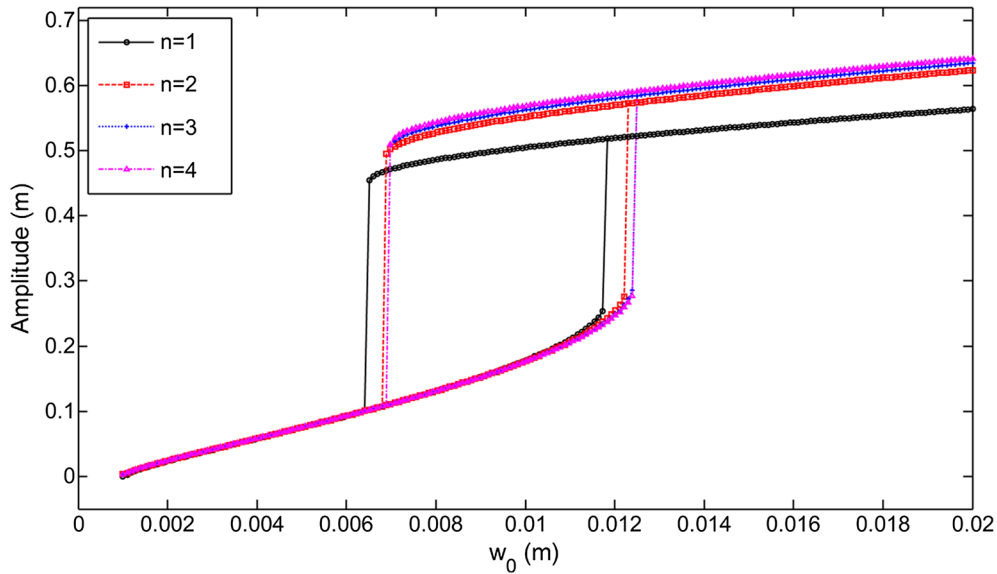


Fig. 8 Force-response curves of the solar array tip with different numbers of modes, $\Omega = 0.42$ Hz

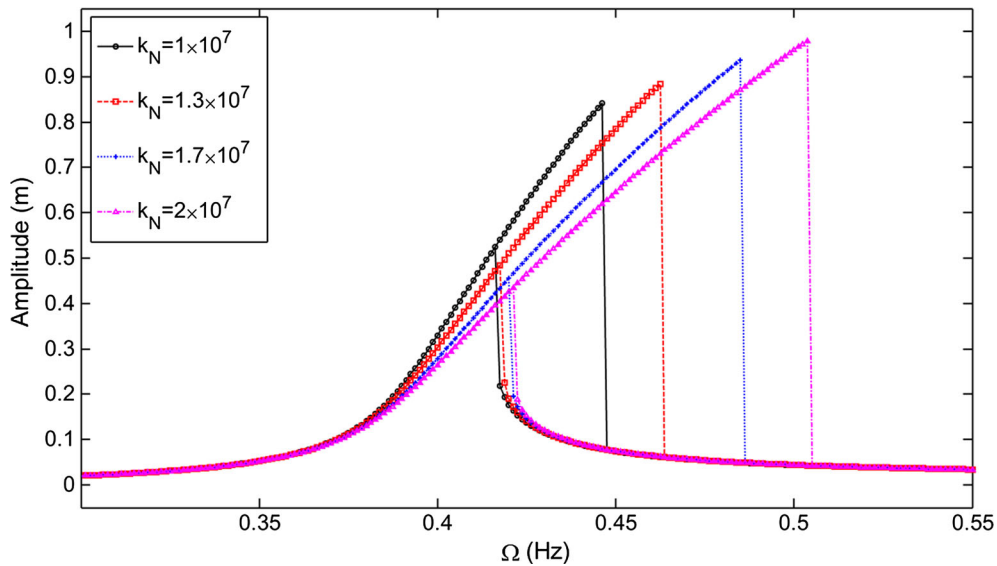


Fig. 9 Frequency-response curves of the solar array tip for various values of k_N , $w_0 = 0.01$ m

are assumed to be zero, and some steady-state response data at the current Ω and w_0 are used as the initial conditions for the next Ω and w_0 , respectively.

When Ω varies from 0.3 to 0.55 Hz, the response curves of the solar array tip for various values of k_N are shown in Fig. 9. From Fig. 9, it can be observed that with the increase in the nonlinear stiffness of the joints, the jump occurs at a higher frequency. In addition, the jump phenomenon is more apparent for a larger k_N .

The response curves for various values of k_N are presented with the frequency of the excitation held fixed $\Omega = 0.42$ Hz when the amplitude of the excitation w_0 is varied from 0.001 to 0.02 m as shown in Fig. 10. It is found that with the increase in the nonlinear stiffness of the joints, the jump occurs at a lower w_0 , and the vibration amplitude of the system decreases.

The frequency-response and force-response curves of the solar array tip for various values of c are shown in Figs. 11 and 12, respectively. From Figs. 11 and 12, it can be observed that in the case of small damping of the joints, obvious jump phenomenon takes place. With the increase in the damping of the joints, this phenomenon

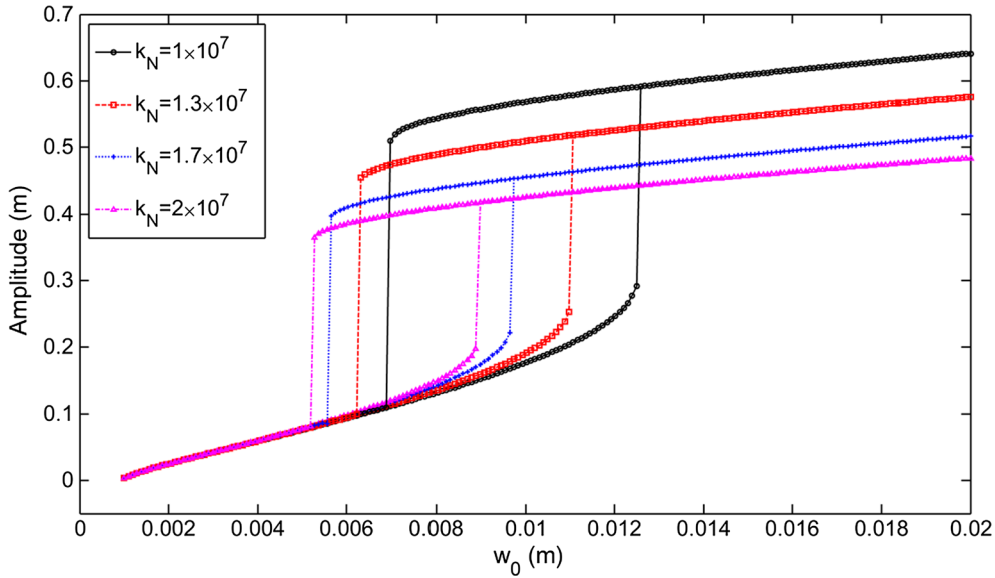


Fig. 10 Force-response curves of the solar array tip for various values of k_N , $\Omega = 0.42$ Hz

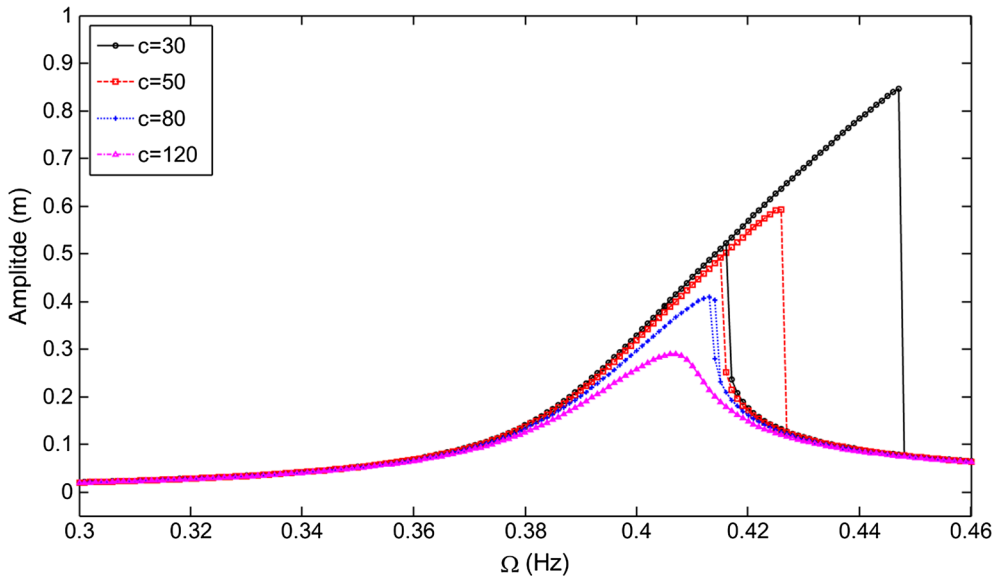


Fig. 11 Frequency-response curves of the solar array tip for various values of c , $w_0 = 0.01$ m

gradually diminished until disappeared. Meanwhile, it is clear that the damping of the joints can reduce the vibration amplitude of the system.

The frequency-response and force-response curves of the solar array tip for various values of μ are shown in Figs. 13 and 14, respectively. From Figs. 13 and 14, it is also found that the friction of the joints can reduce the vibration amplitude of the system. With the increase in the friction of the joints, the jump phenomenon becomes less obvious, and the hysteresis loop becomes smaller as the frequency is increased and decreased. From Figs. 5, 6, 7, 8, 9, 10, 11, 12, 13 and 14, it is concluded that the transmission characteristics of the joints have a great influence on the dynamic behavior of the whole structure.

It is well known that the spacecraft with the solar array is usually extremely flexible and has low-frequency fundamental vibration modes. These modes might be excited in a variety of tasks such as slewing and pointing maneuvers. Thus, damping and friction are simple but effective ways to suppress the induced vibrations. However, in the space environment, solar panels do not provide enough damping to quickly suppress the vibration caused by the maneuvers. Therefore, the overall damping and friction contribution from the joints

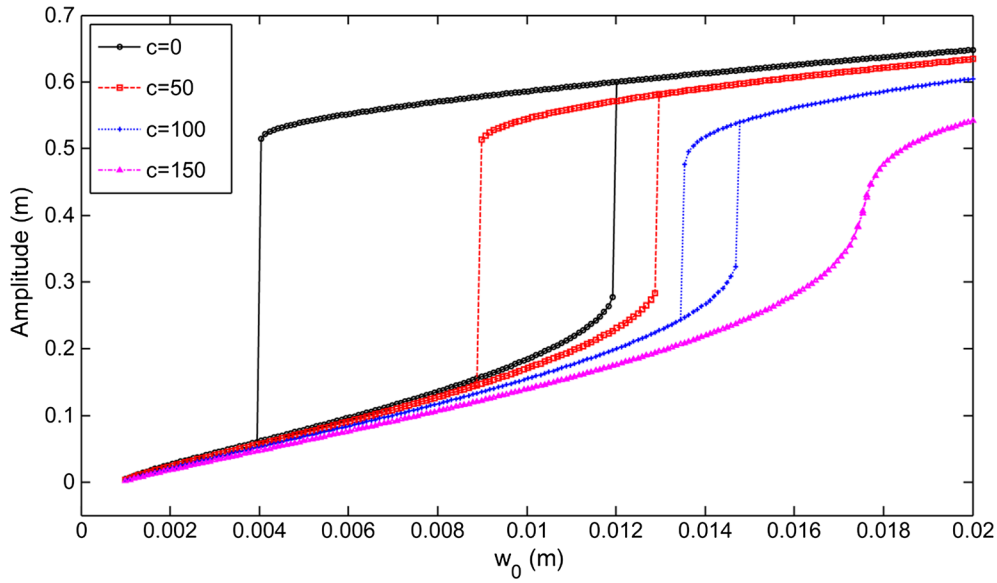


Fig. 12 Force-response curves of the solar array tip for various values of c , $\Omega = 0.42$ Hz

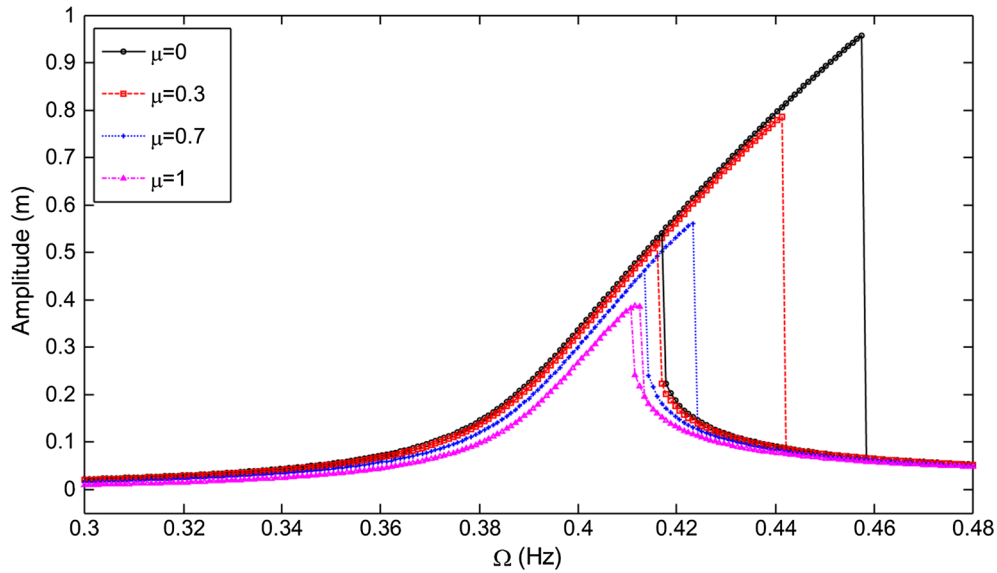


Fig. 13 Frequency-response curves of the solar array tip for various values of μ , $w_0 = 0.01$ m

are very important for suppressing the vibration of the system. In order to investigate the role of the joints in suppressing vibration of the system, the vibration responses of the solar array are carried out. Assume that the external excitation acceleration is

$$\ddot{w}_s(t) = \begin{cases} a, & 0 \leq t \leq T, \\ 0, & t > T. \end{cases} \quad (30)$$

The time history of the external excitation acceleration with $T = 200$ s, $a = 0.2$ m/s² is considered as shown in Fig. 15. When the external and internal damping of the solar panel are selected as $\xi = 0.03$ N s/m and $\eta = 1.9 \times 10^5$ N s/m² as shown in Table 1, the first four modal damping ratios of the solar panel are $\alpha_1 = 0.005$, $\alpha_2 = 0.0059$, $\alpha_3 = 0.0146$ and $\alpha_4 = 0.0279$, respectively. The vibration responses of the solar array tip with different numbers of modes are shown in Fig. 16. From Fig. 16, it can be seen that the model for the first one mode has been unable to calculate the system response accurately, and at least the first two modes should be taken to ensure the accuracy of the system response.

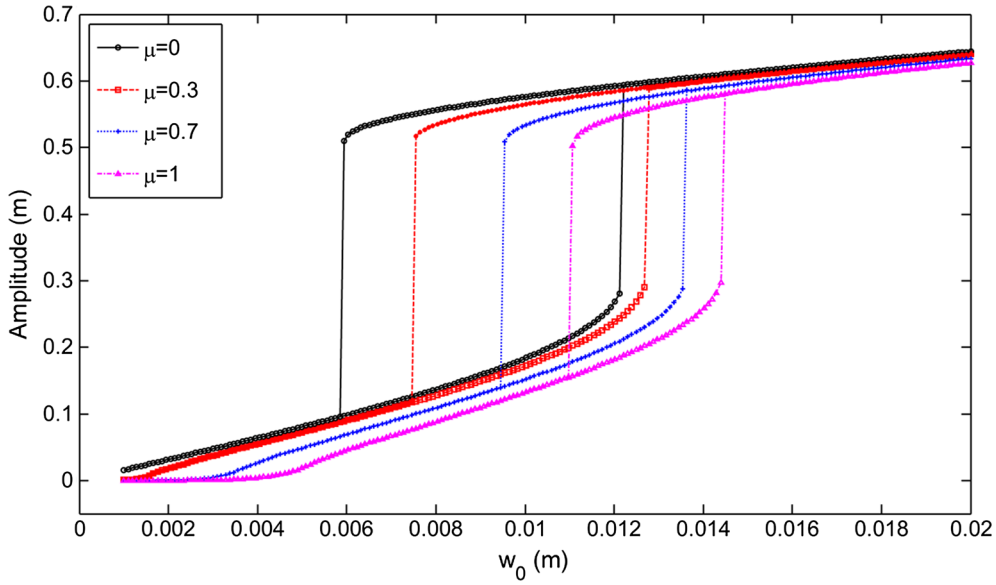


Fig. 14 Force-response curves of the solar array tip for various values of μ , $\Omega = 0.42$ Hz

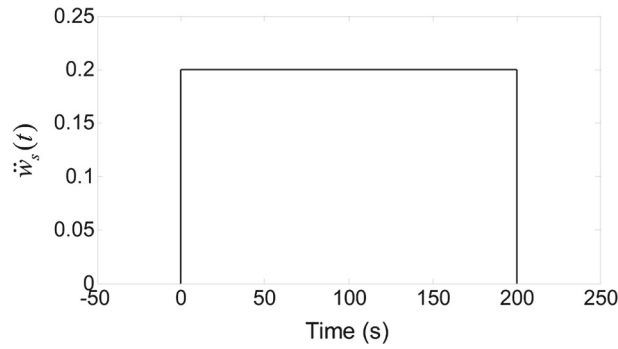


Fig. 15 Time history of external excitation acceleration

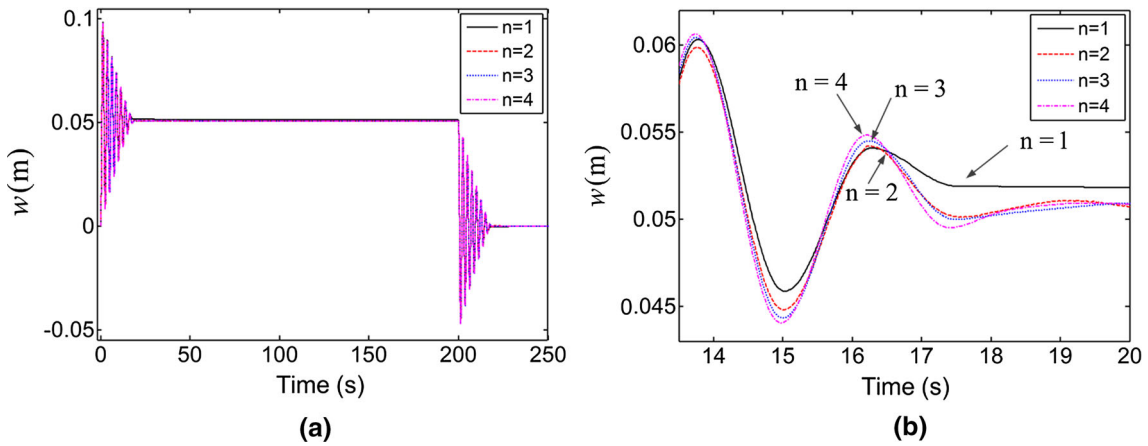


Fig. 16 Responses of the solar array tip with different numbers of modes

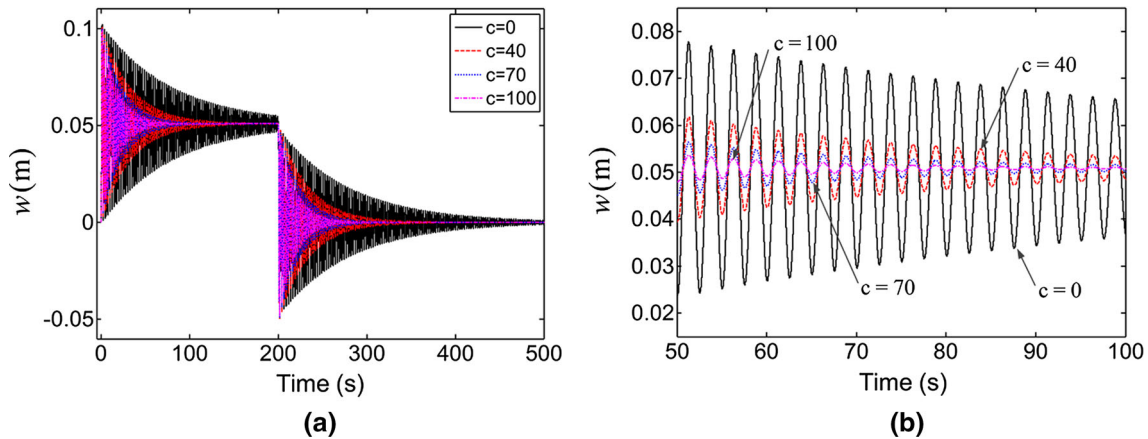


Fig. 17 Responses of the solar array tip for various values of c

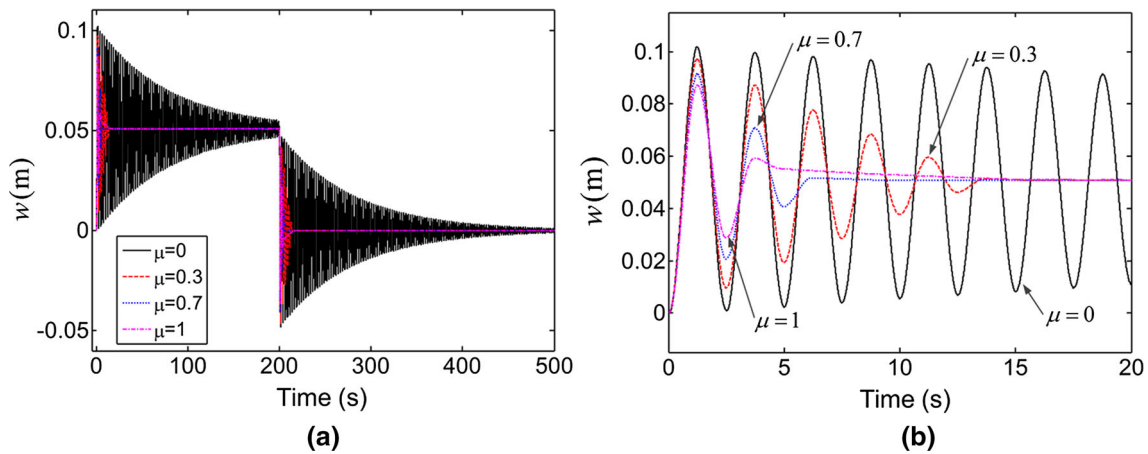


Fig. 18 Responses of the solar array tip for various values of μ

The vibration responses of the solar array tip with the first three modes for various values of c and μ are shown in Figs. 17 and 18, respectively. In Fig. 17, the Coulomb friction torque of the joint is selected as $\mu = 0$ N m. In Fig. 18, the damping of the joint is selected as $c = 0$ N m s/rad. From Figs. 17 and 18, it is clear that with the increase in the damping and friction of the joint, the time of vibration suppression is reduced. In Fig. 17, even if the damping of the joint is selected as $c = 100$ N m s/rad, it also requires 100s to suppress the vibration of the system without the friction of the joint. However, it only needs 14s to suppress the vibration of the system when the friction of the joint is selected as $\mu = 0.3$ N m as shown in Fig. 18. This shows that the friction of the joint is very effective to suppress the vibration of the system.

5 Conclusions

A dynamic modelling approach has been proposed to obtain a reduced-order analytical model for a multi-beam structure considering the nonlinearities in the joints by using the global modes discretization technique. The model formulation presented in this paper is a general one, which can be exploited to obtain an explicit set of nonlinear ODEs for such structures with any number of beams and nonlinear joints. Moreover, the nonlinear dynamic model derived here is not only convenient for solving the system with the analytic method, such as perturbation techniques, but also is preferred to be used for real-time control because fewer DOFs mean less computation time.

Based on the dynamic modelling approach, the flexible structure with 4 beams and nonlinear joints has been presented as an example. Then, a comparison of the natural frequencies has been given to verify the validity of the derived model. Through the nonlinear ODEs of the model, the dynamic responses of the system

with different numbers of modes have been obtained, and the dynamic responses of the system with various joint parameters have been discussed. Two main conclusions are summarized as follows:

- (1) With the increase in the amplitude of the external excitation, due to the effects of the joints nonlinearities, the contribution of the higher-order modes in the response of the system is increased. In the case of large vibration amplitude, the higher-order modes are needed to ensure the accuracy of the response of the system although the external excitation frequency is much smaller than the higher-order natural frequency of the system. In the case of small vibration amplitude, the dynamic equation for the first mode is enough for nonlinear vibration analysis of the system when the external excitation frequency is near the first natural frequency of the system.
- (2) The damping and friction of the joints can increase the stability of the space structure and restrain the vibration of the structure, which are very helpful for the design of vibration sensitive structure.

Acknowledgements This work was supported by the National Natural Science Foundation of China under Grant Nos. 11472089 and 11732005.

Appendix A

The relevant terms in Eq. (28)

$$M_s = \sum_{i=1}^4 \int_{-l}^l \rho [\varphi_i^s(x)]^2 dx, K_s = \sum_{i=1}^4 \int_{-l}^l EI [\varphi_i^{s''}(x)]^2 dx + \sum_{i=1}^4 2k_L [\Theta_i^s]^2, \omega_s^2 = \frac{K_s}{M_s},$$

$$\alpha_s = \frac{1}{2} \left(\frac{\xi}{\rho\omega_s} + \frac{\eta\omega_s}{E} \right), \gamma_s = \frac{1}{M_s} \sum_{i=1}^4 \sum_{j=1}^n 2c\Theta_i^j \Theta_i^s, b_s^j = \frac{1}{M_s} \sum_{i=1}^4 \sum_{j=1}^n 2\mu\Theta_i^s,$$

$$d_s^{jkr} = \frac{1}{M_s} \sum_{i=1}^4 \sum_{j=1}^n \sum_{k=1}^n \sum_{r=1}^n 2k_N \Theta_i^j \Theta_i^k \Theta_i^r \Theta_i^s, f_s(t) = \frac{1}{M_s} \sum_{i=1}^4 \int_{-l}^l \rho \varphi_i^s(x) \ddot{w}_s(t) dx.$$

References

1. Bai, Z.F., Zhao, Y.: Dynamic behaviour analysis of planar mechanical systems with clearance in revolute joints using a new hybrid contact force model. *Int. J. Mech. Sci.* **54**(1), 190–205 (2012)
2. Hunt, K.H., Crossley, F.R.E.: Coefficient of Restitution Interpreted as Damping in Vibroimpact. *J. Appl. Mech. Trans. ASME* **42**(2), 440–445 (1975)
3. Dubowsky, S., Gardner, T.N.: Dynamic Interactions of link elasticity and clearance connections in planar mechanical systems. *J. Eng. Ind. Trans. ASME* **97**(2), 652–661 (1975)
4. Herbert, R.G., Mcwhannell, D.C.: Shape and frequency composition of pulses from an impact pair. *J. Eng. Ind. Trans. ASME* **99**(3), 663–671 (1977)
5. Lankarani, H.M., Nikravesh, P.E.: A contact force model with hysteresis damping for impact analysis of multibody systems. *J. Mech. Des.* **112**(3), 369–376 (1990)
6. Yigit, A.S., Ulsoy, A.G., Scott, R.A.: Spring-dashpot models for the dynamics of a radially rotating beam with impact. *J. Sound Vib.* **142**(3), 515–525 (1990)
7. Liu, R., Zhang, J., Guo, H., Deng, Z.: Experiment and formulations for the dynamic characteristics of jointed structures. *Adv. Mech. Eng.* **2013**(7), 679–681 (2013)
8. Crawley, E.F., Aubert, A.C.: Identification of nonlinear structural elements by force-state mapping. *AIAA J.* **24**(1), 155–162 (1986)
9. Crawley, E.F., O'Donnell, K.J.: Force-state mapping identification of nonlinear joints. *AIAA J.* **25**(7), 1003–1010 (1987)
10. Jalali, H., Ahmadian, H., Mottershead, J.E.: Identification of nonlinear bolted lap-joint parameters by force-state mapping. *Int. J. Solids Struct.* **44**(25), 8087–8105 (2007)
11. Ren, Y., Beards, C.F.: Identification of 'effective' linear joints using coupling and joint identification techniques. *J. Vib. Acoust-Trans. ASME* **120**(2), 331–338 (1998)
12. Ren, Y., Lim, T.M., Lim, M.K.: Identification of properties of nonlinear joints using dynamic test data. *J. Vib. Acoust-Trans. ASME* **120**(2), 324–330 (1998)
13. Gaul, L., Lenz, J.: Nonlinear dynamics of structures assembled by bolted joints. *Acta Mech.* **125**(1), 169–181 (1997)
14. Bowden, M., Dugundji, J.: Joint damping and nonlinearity in dynamics of space structures. *AIAA J.* **28**(4), 740–749 (1990)
15. Quinn, D.D.: Modal analysis of jointed structures. *J. Sound Vib.* **331**(1), 81–93 (2012)
16. Ferri, A.A.: Modeling and analysis of nonlinear sleeve joints of large space structures. *J. Spacecr Rockets* **25**(5), 354–360 (1988)

17. Yoshida, T.: Dynamic characteristic formulations for jointed space structures. *J. Spacecr Rockets* **43**(4), 771–779 (2006)
18. Sarkar, S., Venkatraman, K.: Dynamics of flexible structures with nonlinear joints. *J. Vib. Acoust-Trans. ASME* **126**(1), 92–100 (2004)
19. Mary LB: Dynamics of space structures with nonlinear joints. Massachusetts Institute of Technology, (1988)
20. Wei, F., Zheng, G.T.: Nonlinear vibration analysis of spacecraft with local nonlinearity. *Mech. Syst. Signal Process.* **24**(2), 481–490 (2010)
21. Zhang, J., Guo, H.W., Liu, R.Q., Wu, J., Kou, Z.M., Deng, Z.Q.: Damping formulations for jointed deployable space structures. *Nonlinear Dyn.* **81**(4), 1969–1980 (2015)
22. Silva, : MRMCD: a reduced-order analytical model for the nonlinear dynamics of a class of flexible multi-beam structures. *Int. J. Solids Struct.* **35**(25), 3299–3315 (1998)
23. Wei, J., Cao, D., Liu, L., Huang, W.: Global mode method for dynamic modeling of a flexible-link flexible-joint manipulator with tip mass. *Appl. Math. Model.* **48**, 787–805 (2017)
24. Crawley, E.F.: Nonlinear characteristics of joints as elements of multi-body dynamic systems. NASA Tech. Rep. **N89-24668**, 543–569 (1989)
25. Song, M.T., Cao, D.Q., Zhu, W.D.: Dynamic analysis of a micro-resonator driven by electrostatic combs. *Commun. Nonlinear Sci. Numer.* **16**(8), 3425–3442 (2011)
26. Cao, D.Q., Song, M.T., Zhu, W.D., Tucker, R.W., Wang, H.T.: Modeling and analysis of the in-plane vibration of a complex cable-stayed bridge. *J. Sound Vib.* **331**(26), 5685–5714 (2012)
27. Wei, J., Cao, D., Wang, L., Huang, H., Huang, W.: Dynamic modeling and simulation for flexible spacecraft with flexible jointed solar panels. *Int. J. Mech. Sci.* **130**, 558–570 (2017)
28. Clough, R.W., Penzien, J.: *Dynamics of Structures*. McGraw-Hill, New York (1975)
29. Liu, L., Cao, D., Tan, X.: Studies on global analytical mode for a three-axis attitude stabilized spacecraft by using the Rayleigh-Ritz method. *Arch. Appl. Mech.* **86**(12), 1–20 (2016)